

RSC Advances



This is an *Accepted Manuscript*, which has been through the Royal Society of Chemistry peer review process and has been accepted for publication.

Accepted Manuscripts are published online shortly after acceptance, before technical editing, formatting and proof reading. Using this free service, authors can make their results available to the community, in citable form, before we publish the edited article. This *Accepted Manuscript* will be replaced by the edited, formatted and paginated article as soon as this is available.

You can find more information about *Accepted Manuscripts* in the [Information for Authors](#).

Please note that technical editing may introduce minor changes to the text and/or graphics, which may alter content. The journal's standard [Terms & Conditions](#) and the [Ethical guidelines](#) still apply. In no event shall the Royal Society of Chemistry be held responsible for any errors or omissions in this *Accepted Manuscript* or any consequences arising from the use of any information it contains.



COMMUNICATION

Facile Synthesized Highly Active Pd Nanoparticle Electrocatalyst for Electroless Deposition Process

Received 00th January 20xx,
Accepted 00th January 20xx

Desmond C. L. Tan,^a Bahareh Khezri,^b Wannipha Amatyakul,^c Richard D. Webster^b and Hirotaka Sato^a

DOI: 10.1039/x0xx00000x

www.rsc.org/

Pd nanoparticles chemically synthesized by respective reducing agents were evaluated in the hypophosphite oxidation reaction for initiating electroless Ni deposition. The P co-deposited Pd nanoparticles exhibited competitively high specific activity as conventional Pd nanoparticles synthesized by tin (II) chloride while having superior mass activity and simplicity in the deposition process.

Electroless deposition, being the reduction of metal ions by electrons charged not from an external power source but from reducing agents co-existing in the solution, has been employed as an advanced metallization technology for thin film¹⁻³ (atomic layer to sub-millimeter range), nano-structure fabrication^{4,5}, modifying micro/nano-structures^{6,7} and even substrate patterning⁸. Advances on electroless Ni deposition are of great interest due to its wide application^{9,10}. The fundamental electroless deposition process steps are; (1) a solid substrate is functionalized with Pd nanoparticles which work as the catalyst for the oxidation of hypophosphite, and (2) the substrate is dipped into the solution containing metal ions (example Ni ions) and reducing agent (example hypophosphite is popularly used). In step (2), hypophosphite is oxidised initially on the Pd nanoparticles and discharges electrons which are received by Ni ion to deposit as Ni metal. Once Ni is deposited, the Ni deposition proceeds continuously as the Ni metal surface itself works as a catalyst for the oxidation of hypophosphite.

The Pd catalyst deposited at step (1) is a cost barrier to the widespread use of the electroless deposition process because the Pd market price is considerably high and step (1) needs multiple chemical-wasting procedures. SnCl₂ has been

traditionally used as the reducing agent to yield Pd nanoparticles (here, let Pd-Sn denote the Pd nanoparticle catalyst synthesized by SnCl₂). Pd-Sn nanoparticles deposited on a solid surface substrate by stepwise dipping of the substrate into PdCl₂ and SnCl₂ solutions sequentially, is a conventionally used catalyst for initiating electroless Ni deposition^{11,12}. However, the stability of the SnCl₂ solution is poor due to chemical reactions which may occur such as hydrolysis or Sn (II) and Sn (IV) complex formation^{13,14}, resulting in a large volume of waste or extra expenses in tin recovery^{15,16}. Furthermore, the Pd-Sn catalyst needs 'acceleration treatment', where the Pd-Sn deposited substrate is dipped in an acid or alkaline solution to remove tin oxide, an unreactive composition in Pd-Sn, and expose more Pd reactive sites for hypophosphite oxidation¹⁷. The acceleration treatment is expensive as the acceleration solution needs to be frequently monitored so that renewal of solution can be performed immediately to ensure the consistency in the acceleration treatment. In addition, not only tin oxide but also some amount of Pd are removed and lost in the process. Hence, alternative procedures are needed to deposit Pd nanoparticles which may be more stable and simple (without any acceleration treatment) while having as high catalytic activity as Pd-Sn.

In the present work, the catalytic activities of Pd nanoparticle electrocatalysts synthesized by different reducing agents were investigated to seek replacement of SnCl₂ while achieving as high an activity as the Pd nanoparticles synthesized by SnCl₂. These synthesized Pd nanoparticles do not require the acceleration treatment for enhancing their catalytic activity.

The Pd nanoparticle electrocatalysts were synthesized on a glassy carbon (GC) electrode with the respective reducing agents – sodium hypophosphite for Pd-P, hydrazine hydrate for Pd-N₂H₄ or SnCl₂ (See Experimental details in ESI†)¹⁸. Field emission scanning electron microscopy (FESEM, JEOL JSM-7600F) and transmission electron microscopy (TEM, JEOL JEM-2010 microscope operated at 200 kV) were used to observe the synthesized Pd nanoparticles. Cyclic voltammetry (CV) and

^aSchool of Mechanical & Aerospace Engineering, Nanyang Technological University, 50 Nanyang Avenue, Singapore 639798

^bDivision of Chemistry & Biological Chemistry, School of Physical and Mathematical Sciences, Nanyang Technological University, 21 Nanyang Link, Singapore 637371

^cResearch & Development, Okuno-Auromex (Thailand) Co., Ltd, 23 Soi Saladaeng 1, Rama IV Road, Silom, Bangrak, Bangkok 10500 Thailand

†Electronic Supplementary Information (ESI) available: [details of any supplementary information available should be included here]. See DOI: 10.1039/x0xx00000x

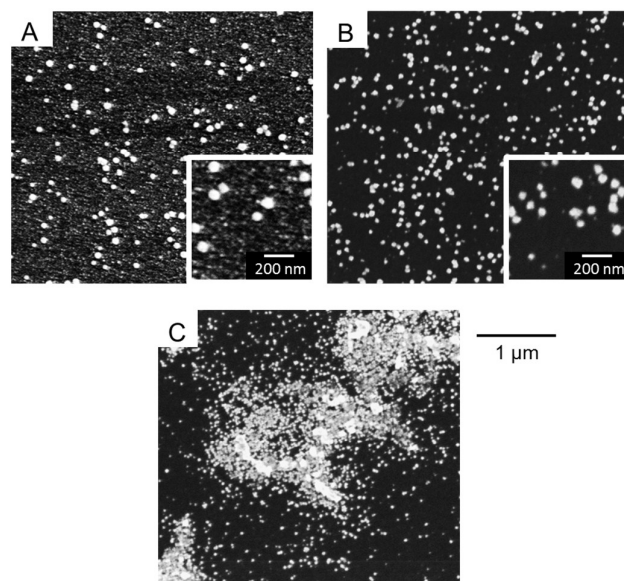


Fig. 1 SEM images of (A) Pd-P, (B) Pd-N₂H₄ and (C) Pd-Sn/AA.

induction time (time interval from the beginning of electrode dipping into the solution to the beginning of the metal deposition¹⁹) experiments were performed to evaluate the catalytic performance in oxidizing hypophosphite.

The synthesized Pd-P nanoparticles are well dispersed with a combination of small (~5 nm) and large (~50 nm) nanoparticles (Fig. 1A). The electron diffraction pattern (Fig. S5 ESI[†]) is relatively halo indicating the Pd nanoparticles are partially amorphous or disordered microstructures, which should be due to the phosphorus co-deposited into the nanoparticles^{20,21} (Fig. S4 ESI[†]). For Pd-N₂H₄ (Fig. 1B), the nanoparticles are also well dispersed and the electron diffraction pattern shows clear Debye-Scherrer rings indicating that the Pd-N₂H₄ nanoparticles are crystalline. On the other hand, Pd-Sn nanoparticles after acceleration, Pd-Sn/AA (Fig. 1C) are small but they are prone to coagulation. From the SEM image, the Pd-Sn nanoparticles are found to be concealed under some materials and the EDS result (Fig. S3 ESI[†]) suggests that these materials are tin/tin-complexes. Further investigation with XRD (Fig. S4 ESI[†]) shows that tin oxide complexes are still present after acceleration treatment. Hence, the above observations imply that the acceleration treatment could not completely remove the tin oxide complexes, leaving part of the Pd-Sn nanoparticles unexposed. Note that longer acceleration treatment might be able to remove the tin oxide complex further but results in the loss of Pd-Sn catalyst as well²². The electron diffraction pattern shows that Pd-Sn/AA nanoparticles are crystalline which is in agreement with the result of Osaka and Nagasaka²³.

CV of the Pd-P electrocatalyst was conducted and shown in Fig. 2. The presence of hypophosphite in solution significantly changes the shape of the CVs. In the presence of hypophosphite, the CV shows a slight hump (P1) at approximately -0.20 V vs. Ag/AgCl followed by a broad peak (P2) at approximately 0.04 V while the backward scan shows

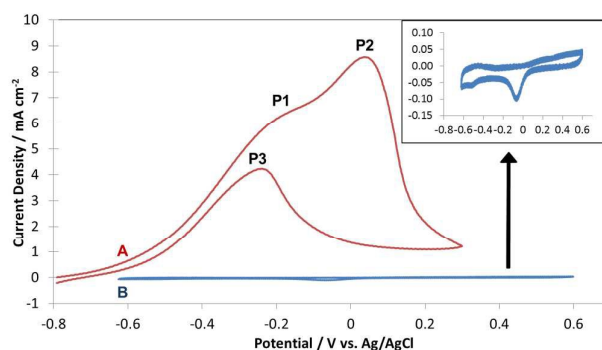


Fig. 2 Cyclic voltammograms of Pd-P in the solutions with (A) and without (B) NaH₂PO₂. Scan rate 50 mV s⁻¹. The inset is an enlarged scale of (B). CV of Pd-P in solution with NaH₂PO₂ (Fig. 2A) shows the 3 broad peaks which is absence in the CV without NaH₂PO₂ (Fig. 2B). The measured currents are normalised by geometric area of electrode.

an anodic peak (P3) at -0.23 V (Fig. S1, ESI[†] shows CV for bare GC where no peak and negligible current were observed). The result indicates that P1, P2 and P3 correspond to the oxidation of hypophosphite in the solution. According to literature^{24,25}, P1 is attributed to hypophosphite oxidation in the solution while P2 correspond to the simultaneous reaction of hypophosphite oxidation and palladium ionization. The CV without NaH₂PO₂ (blue) shows that the current output from palladium ionization is negligible, so the current output of P2 is likely to be a contribution of hypophosphite oxidation only. P3 is observed in the reverse scan at very negative potentials due to the high catalytic activity of palladium and the irreversibility of the hypophosphite oxidation^{24,26}. The specific and mass activities of the electrocatalysts were calculated from the peak current of the respective P2 peaks.

The CVs for Pd-Sn before and after the acceleration treatment in the absence of hypophosphite are shown in Fig. S2 (ESI[†]). The acceleration treatment exposes Pd reactive sites for hypophosphite oxidation as the PdO reduction peak can be observed only after the treatment. According to Osaka and Nagasaka²³, the acceleration treatment removes the stannous and stannic oxides and hydroxides on the surface and exposes the bare active Pd nuclei. This was verified by XRD of Pd-Sn before and after the acceleration treatment (Fig. S3 ESI[†]) as the Pd peak can be seen only after acceleration treatment.

The CVs in the presence of hypophosphite with various electrocatalysts that were normalized by electrochemical active surface area (ECSA, see ESI[†]) and Pd loads are shown in Fig. 3 shows the specific and mass activities for the oxidation of hypophosphite. In Fig. 3A, the specific activity for Pd-Sn before acceleration was not included as the ECSA of Pd nanoparticles was not computable with the negligible PdO reduction peak (shown in Fig. S2 ESI[†]). The average peak specific activity of Pd-P, Pd-N₂H₄ and Pd-Sn/AA are 23.8, 13.8 and 34.8 mA cm⁻² respectively. Pd-Sn/AA electrocatalyst exhibited higher specific activity compared to Pd-N₂H₄ indicates that the bimetallic interaction by having Sn incorporating into Pd has a positive effect on the catalytic

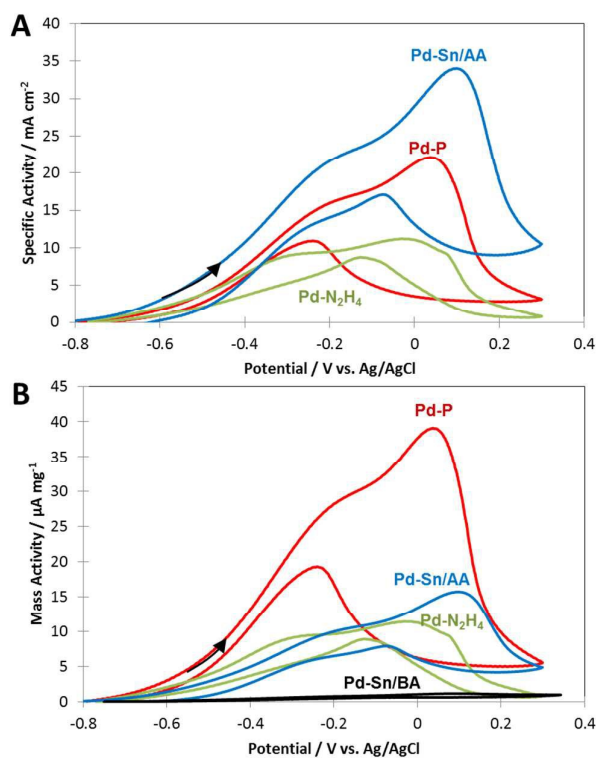


Fig. 3 Cyclic voltammograms of various Pd nanoparticle electrocatalysts in solution (pH 9) with NaH_2PO_2 normalized by (A) electrochemically active surface area (specific activity) and (B) Pd load (mass activity). Scan rate is 50 mV s^{-1} . Pd-Sn exhibits the highest specific activities while Pd-P mass activities for the anodic (forward) polarisation sweep among all electrocatalysts.

properties. This is in agreement with other studies showing that bimetallic catalysts work better than mono-metal catalysts^{27,28}. The Pd-P electrocatalyst has higher specific activity compared to Pd-N₂H₄; this may be associated to the electronic effect between Pd and P when small amount of phosphorus (verified EDX in Fig. S4 ESI[†]) was doped in the Pd lattice²⁹⁻³¹. Another contributing factor could be due to the partially amorphous or disordered microstructure of Pd-P. Lower degree of crystallinity is likely to have more abundant defects, kinks and edges resulting in more low coordination sites. These low coordination sites are proven to have higher catalytic activity^{18,32}.

The mass activities, the current normalized by the load of the precious metal (Pd in this study), of Pd-P, Pd-N₂H₄ and Pd-Sn electrocatalysts were compared as shown in Fig. 3B. The average peak mass activity of Pd-P, Pd-N₂H₄, Pd-Sn/BA and Pd-Sn/AA are 38.7, 10.5, 1.3 and 14.5 $\mu\text{A mg}^{-1}$ respectively. Pd-P electrocatalyst has remarkably higher mass activity compared to others. Pd-Sn electrocatalyst exhibited low mass activity possibly due to the surface having significant amount of reactive sites blocked by tin oxides (not removed by the acceleration treatment) overlay (shown in XRD Fig. S3 ESI[†]) and subsequently resulted in poor adsorption of H_2PO_2^- on the Pd nanoparticles. This means that much of the Pd-Sn nanoparticles were embedded (wasted) under the tin oxide

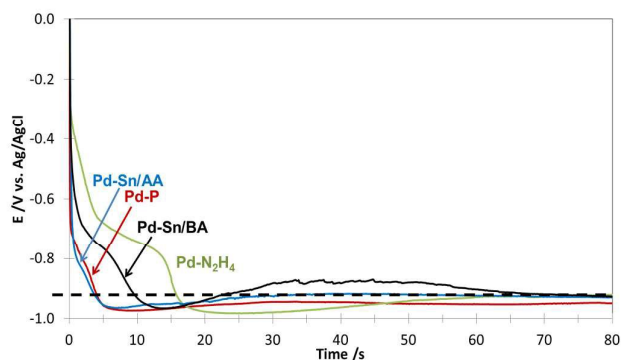


Fig. 4 Open circuit potentials of Pd electrocatalysts deposited electrodes as immersed in a Ni electroless deposition bath (pH 9) at 60°C . The sampling rate is 10 pts s^{-1} . Pd-P and Pd-Sn show the shortest induction time to reach steady-state mixed potential (black dashed line), followed Pd-N₂H₄.

complexes and not participating in the oxidation process, causing the substantially poor mass activity. The mass activity for Pd-Sn/AA was noticeably higher compared to Pd-Sn/BA due to the increase in Pd-Sn nanoparticles exposed after tin oxides removal. Even with significant removal of tin oxides layer, Pd-Sn/AA still has considerably low mass activity due to coagulation of nanoparticles and the un-removed tin oxides which blocks the reactive sites for hypophosphite oxidation. It was observed that Pd-P exhibited substantially higher mass activity compared to Pd-N₂H₄. This is probably due to the considerably higher loading of smaller nanoparticles ($\sim 5 \text{ nm}$) in Pd-P than Pd-N₂H₄ shown in the inset of Fig. 1. This implies that Pd-P nanoparticles have more reactive sites for H_2PO_2^- oxidation and therefore significantly enhanced the oxidising capability compared to Pd-N₂H₄. Furthermore, Pd-P and Pd-Sn/AA showing superior mass activity compared to Pd-N₂H₄ can be possibly contributed by the substantially higher specific activity as in Fig. 3A. Thus, the specific and mass activity showed that Pd-P electrocatalyst has competitive activity and higher cost-effectivity when compared with Pd-Sn/AA electrocatalyst.

The open-circuit potential (OCP) measurements of the Pd electrocatalysts when immersed in the nickel bath solution at 60°C ^{33,34} are shown in Fig. 4. The induction period is defined as the time needed for the OCP to reach the mixed potential (E_{mp}) where steady-state deposition commence, based on Paunovic's study on electroless copper deposition¹⁹. The electrocatalysts are considered active for electroless nickel deposition if their OCP reaches E_{mp} ³⁵, thus the time taken to establish E_{mp} signify the catalytic activity of the electrocatalysts³⁴. From Fig. 4, the E_{mp} is estimated to be around $-0.94 \text{ V vs Ag/AgCl}$. Pd-Sn/AA (4.3 s) and Pd-P (4.5 s) have the lowest induction time compared to Pd-Sn/BA (10.4 s) and Pd-N₂H₄ (16.3 s), showing that the activity in hypophosphite oxidation is in the order of Pd-Sn/AA \approx Pd-P $>$ Pd-N₂H₄³⁴. The OCP result is in agreement with the specific and mass activity result indicating that Pd-N₂H₄ has the worst performance among the three electrocatalysts³⁴ and acceleration improved the catalytic activity for Pd-Sn. Both

results showed that Pd-Sn/AA and Pd-P electrocatalysts have comparable activity, but because of the tin oxides layer blocking reactive sites coagulation of Pd-Sn nanoparticles, Pd-Sn/AA has lower cost-effectiveness (lower mass activity) than Pd-P. Possibly, with some improved deposition method or acceleration treatment in achieving monolayers of the Pd-Sn electrocatalyst, Pd-Sn nanoparticles may result in enhanced cost-effectiveness. However, St. John *et al.* showed that the extension of the acceleration treatment led to loss of noble metal on the electrode surface from their attempt to accomplish further removal of the tin oxides²². On the other hand, it is noted that Pd-P exhibits competitive specific activity and the highest mass activity, and it also does not require any acceleration treatment unlike Pd-Sn which makes the deposition process simpler and less expensive. This makes Pd-P a more preferable electrocatalyst compared to Pd-Sn.

In conclusion, Pd nanoparticle electrocatalysts synthesized by different reducing agents were evaluated for their catalytic activity for hypophosphite oxidation. Pd-P has higher cost-effectiveness compared to Pd-Sn and Pd-N₂H₄. Moreover, Pd-P does not require the acceleration treatment unlike Pd-Sn. Overall, Pd-P is a potential candidate to substitute Pd-Sn in the electroless deposition process.

This work was supported by the Nanyang Assistant Professorship (NAP, M4080740), Singapore Ministry of Education (MOE2013-T2-2-049) and Okuno-Auromex Co Ltd. The authors appreciate Ms. Koh Joo Luang, Ms. Yong Mei Yoke and Mr. Leong Kwok Phui, Materials Laboratories at MAE, NTU, for their continuous effort to set up and maintain an excellent experimental environment.

Notes and references

- L. M. Luo, Z. L. Lu, X. M. Huang, X. Y. Tan, X. Y. Ding, J. G. Cheng, L. Zhu and Y. C. Wu, *Surf. Coat. Technol.*, 2014, **251**, 69-73.
- Y. Yu, C. Yan and Z. J. Zheng, *Adv. Mater.*, 2014, **26**, 5508-5516.
- K. Banu and T. Shimura, *New J. Chem.*, 2011, **35**, 1503-1514.
- P. C. Hsu, D. S. Kong, S. Wang, H. T. Wang, A. J. Welch, H. Wu and Y. Cui, *J. Am. Chem. Soc.*, 2014, **136**, 10593-10596.
- K. D. Beard, D. Borrelli, A. M. Cramer, D. Blom, J. W. Van Zee and J. R. Monnier, *ACS Nano*, 2009, **3**, 2841-2853.
- I. Lee, P. T. Hammond and M. F. Rubner, *Chem. Mat.*, 2003, **15**, 4583-4589.
- A. M. Bazargan, S. Ghashghai, M. Keyanpour-rad and M. E. Ganji, *RSC Adv.*, 2012, **2**, 1842-1845.
- A. Garcia, J. Polesel-Maris, P. Viel, S. Palacin and T. Berthelot, *Adv. Funct. Mater.*, 2011, **21**, 2096-2102.
- A. Agarwal, M. Pujari, R. Uppaluri and A. Verma, *Ultrason. Sonochem.*, 2014, **21**, 1382-1391.
- C. H. Chen, B. H. Chen and L. Hong, *Chem. Mat.*, 2006, **18**, 2959-2968.
- M. Garcia-Gabaldon, V. Perez-Herranz, J. Garcia-Anton and J. L. Guinon, *J. Appl. Electrochem.*, 2007, **37**, 1145-1152.
- R. H. Guo, S. X. Jiang, C. W. M. Yuen, M. C. F. Ng and J. W. Lan, *Fiber. Polym.*, 2013, **14**, 459-464.
- H. Monien, *J. Electroanal. Chem.*, 1969, **20**, 119-8.
- J. Przyluski, M. Kasprzak and J. Bielinski, *Surf. Coat. Technol.*, 1987, **31**, 203-211.
- M. Garcia-Gabaldon, V. Perez-Herranz, J. Garcia-Anton and J. L. Guinon, *Sep. Purif. Technol.*, 2005, **45**, 183-191.
- M. Garcia-Gabaldon, V. Perez-Herranz, J. Garcia-Anton and J. L. Guinon, *Sep. Purif. Technol.*, 2006, **51**, 143-149.
- R. L. Cohen and K. W. West, *J. Electrochem. Soc.*, 1973, **120**, 502-508.
- K. C. Poon, D. C. L. Tan, T. D. T. Vo, B. Khezri, H. B. Su, R. D. Webster and H. Sato, *J. Am. Chem. Soc.*, 2014, **136**, 5217-5220.
- M. Paunovic, *J. Electrochem. Soc.*, 1977, **124**, 349-354.
- L. M. Abrantes, A. Fundo and G. Jin, *J. Mater. Chem.*, 2001, **11**, 200-203.
- P. S. Kumar and P. K. Nair, *J. Mater. Sci. Lett.*, 1994, **13**, 671-674.
- S. St John, D. Lee, I. Dutta and A. Angelopoulos, *J. Electrochem. Soc.*, 2010, **157**, B1245-B1250.
- T. Osaka, H. Nagasaka and F. Goto, *J. Electrochem. Soc.*, 1980, **127**, 2343-2346.
- G. V. Khaldeev, I. V. Petukhov and M. G. Shcherban, *Russ. J. Electrochem.*, 2000, **36**, 934-941.
- J. J. Podesta, R. C. V. Piatti and A. J. Arvia, *J. Appl. Electrochem.*, 1990, **20**, 245-251.
- L. M. Abrantes, M. C. Oliveira, J. P. Bellier and J. Lecoeur, *Electrochim. Acta*, 1994, **39**, 1915-1922.
- D. S. Wang and Y. D. Li, *Adv. Mater.*, 2011, **23**, 1044-1060.
- D. B. Huang, Q. Yuan, H. H. Wang and Z. Y. Zhou, *Chem. Commun.*, 2014, **50**, 13551-13554.
- R. Rego, A. M. Ferraria, A. M. B. do Rego and M. C. Oliveira, *Electrochim. Acta*, 2013, **87**, 73-81.
- J. F. Zhang, Y. Xu and B. Zhang, *Chem. Commun.*, 2014, **50**, 13451-13453.
- L. F. Cheng, Z. H. Zhang, W. X. Niu, G. B. Xu and L. D. Zhu, *J. Power Sources*, 2008, **182**, 91-94.
- F. Y. Cheng, J. A. Shen, B. Peng, Y. D. Pan, Z. L. Tao and J. Chen, *Nat. Chem.*, 2011, **3**, 79-84.
- I. Ohno, O. Wakabayashi and S. Haruyama, *J. Electrochem. Soc.*, 1985, **132**, 2323-2330.
- D. Tian, N. Li, N. Xiao, F. F. Wang, S. Y. Yu, Q. Li, W. Gao and G. Wu, *J. Electrochem. Soc.*, 2013, **160**, D95-D101.
- L. M. Abrantes and J. P. Correia, *J. Electrochem. Soc.*, 1994, **141**, 2356-2360.

